

Article

Research on Molecular Structure and Electronic Properties of Ln^{3+} (Ce^{3+} , Tb^{3+} , Pr^{3+})/ Li^+ and Eu^{2+} Co-Doped $\text{Sr}_2\text{Si}_5\text{N}_8$ via DFT Calculation

 Ziqian Yin ¹, Meijuan Li ^{1,2,*}, Jianwen Zhang ¹ and Qiang Shen ^{1,*}

¹ State Key Laboratory of Advanced Technology for Materials Synthesis and Processing, Wuhan University of Technology, Wuhan 430070, China; yinziqian1996@163.com (Z.Y.); elliott@whut.edu.cn (J.Z.)

² School of Chemistry, Chemical Engineering and Life Sciences, Wuhan University of Technology, Wuhan 430070, China

* Correspondence: meijuanli@whut.edu.cn (M.L.); sqqf@263.net (Q.S.)

Abstract: We use density functional theory (DFT) to study the molecular structure and electronic band structure of $\text{Sr}_2\text{Si}_5\text{N}_8:\text{Eu}^{2+}$ doped with trivalent lanthanides ($\text{Ln}^{3+} = \text{Ce}^{3+}, \text{Tb}^{3+}, \text{Pr}^{3+}$). Li^+ was used as a charge compensator for the charge imbalance caused by the partial replacement of Sr^{2+} by Ln^{3+} . The doping of Ln lanthanide atom causes the structure of $\text{Sr}_2\text{Si}_5\text{N}_8$ lattice to shrink due to the smaller atomic radius of Ln^{3+} and Li^+ compared to Sr^{2+} . The doped structure's formation energy indicates that the formation energy of Li^+ , which is used to compensate for the charge imbalance, is the lowest when the Sr2 site is doped. Thus, a suitable Li^+ doping site for double-doped lanthanide ions can be provided. In $\text{Sr}_2\text{Si}_5\text{N}_8:\text{Eu}^{2+}$, the doped Ce^{3+} can occupy partly the site of Sr_1^{2+} ($[\text{SrN}_8]$), while Eu^{2+} accounts for Sr_1^{2+} and Sr_2^{2+} ($[\text{SrN}_{10}]$). When the Pr^{3+} ion is selected as the dopant in $\text{Sr}_2\text{Si}_5\text{N}_8:\text{Eu}^{2+}$, Pr^{3+} and Eu^{2+} would replace Sr_2^{2+} simultaneously. In this theoretical model, the replacement of Sr^{2+} by Tb^{3+} cannot exist reasonably. For the electronic structure, the energy level of $\text{Sr}_2\text{Si}_5\text{N}_8:\text{Eu}^{2+}/\text{Li}^+$ doped with Ce^{3+} and Pr^{3+} appears at the bottom of the conduction band or in the forbidden band, which reduces the energy bandgap of $\text{Sr}_2\text{Si}_5\text{N}_8$. We use DFT+U to adjust the lanthanide ion 4f energy level. The adjusted 4f-CBM of $\text{Ce}_{\text{Sr}_1}\text{Li}_{\text{Sr}_1}\text{-Sr}_2\text{Si}_5\text{N}_8$ is from 2.42 to 2.85 eV. The energy range of 4f-CBM in $\text{Pr}_{\text{Sr}_1}\text{Li}_{\text{Sr}_1}\text{-Sr}_2\text{Si}_5\text{N}_8$ is 2.75–2.99 eV and its peak is 2.90 eV; the addition of Ce^{3+} in $\text{Eu}_{\text{Sr}_1}\text{Ce}_{\text{Sr}_1}\text{Li}_{\text{Sr}_1}$ made the 4f energy level of Eu^{2+} blue shift. The addition of Pr^{3+} in $\text{Eu}_{\text{Sr}_2}\text{Pr}_{\text{Sr}_2}\text{Li}_{\text{Sr}_1}$ makes part of the Eu^{2+} 4f energy level blue shift. Eu^{2+} 4f energy level in $\text{Eu}_{\text{Sr}_2}\text{Ce}_{\text{Sr}_1}\text{Li}_{\text{Sr}_1}$ is not in the forbidden band, so Eu^{2+} is not used as the emission center.

Keywords: first principles; density functional theory calculations; electronic structure; photoluminescence material; $\text{Sr}_2\text{Si}_5\text{N}_8:\text{Eu}^{2+}$



Citation: Yin, Z.; Li, M.; Zhang, J.; Shen, Q. Research on Molecular Structure and Electronic Properties of Ln^{3+} (Ce^{3+} , Tb^{3+} , Pr^{3+})/ Li^+ and Eu^{2+} Co-Doped $\text{Sr}_2\text{Si}_5\text{N}_8$ via DFT Calculation. *Molecules* **2021**, *26*, 1849. <https://doi.org/10.3390/molecules26071849>

Academic Editor: Jürgen Köhler

Received: 2 March 2021

Accepted: 21 March 2021

Published: 25 March 2021

Publisher's Note: MDPI stays neutral with regard to jurisdictional claims in published maps and institutional affiliations.



Copyright: © 2021 by the authors. Licensee MDPI, Basel, Switzerland. This article is an open access article distributed under the terms and conditions of the Creative Commons Attribution (CC BY) license (<https://creativecommons.org/licenses/by/4.0/>).

1. Introduction

Red fluorescent materials are essential parts of improving the color rendering index in phosphor-converted WLEDs (pc-WLEDs) and have high application value. With rare-earth ions as activating ions, as a representative of the matrix of red phosphors, $\text{Sr}_2\text{Si}_5\text{N}_8$ alkaline earth metal silicon nitride has been extensively studied in recent years [1–3]. When Eu^{2+} is used as the activating ion, the luminous intensity is the highest. Simultaneously, $\text{Sr}_2\text{Si}_5\text{N}_8:\text{Eu}^{2+}$ has become the representative of commercial red fluorescent materials because of its outstanding fluorescence performance in all aspects [4]. However, the main problem is that $\text{Sr}_2\text{Si}_5\text{N}_8:\text{Eu}^{2+}$ is sensitive to temperature, and $\text{Sr}_2\text{Si}_5\text{N}_8:\text{Eu}^{2+}$ luminous intensity is significantly reduced when the temperature is higher. Considering that $\text{M}_2\text{Si}_5\text{N}_8$ is a layered or similar layered structure, its openness is relatively high so that the above problems can be solved through component engineering [5].

The coordination environment, electronic structure, and morphological characteristics of the Eu^{2+} ion are several vital factors that affect phosphors' luminescence performance.

They determine the luminescence characteristics by indirectly changing the degree of crystal field splitting (CFS) [6], nephelauxetic effect (NE), the highest and lowest 5d energy level splitting [7,8]. For example, from both experiments and calculations Li [9] and Bulloni [10] proved that Ca^{2+} partially replaced Eu^{2+} in $\text{Sr}_2\text{Si}_5\text{N}_8$ matrix's emission peaks, which tended to appear red-shifted in Eu^{2+} occupied eight coordination sites, though its stability was reduced. Liu used Ba^{2+} to replace partial Sr^{2+} in $\text{Sr}_2\text{Si}_5\text{N}_8$, after the substitution, the emission peak was blue-shifted. As Eu^{2+} in the ten-coordinate structure is more stable than the eight-coordinate structure, its thermal stability is improved. Chen [11] performed a doping modification based on $\text{Sr}_2\text{Si}_5\text{N}_8:\text{Eu}^{2+}$. In $\text{Sr}_2\text{Si}_5\text{N}_8:\text{Eu}^{2+}$, part of Al^{3+} is used to replace Si^{4+} . As the Al-N bond length is longer than that of Si-N, the bond length between Eu^{2+} and surrounding N^{3-} is shorter, the crystal field intensity increases, and the emission peak position is red-shifted. Wang [12] used partial AlO^+ instead of SiN^+ , and the effects of the increase in the crystal field and the increase in electronegativity cancelled each other out, rendering the peak position unchanged, but the thermal stability and strength increased. In $\text{Rb}_3\text{Ysi}_2\text{O}_7:\text{Eu}^{2+}$ system, the weak covalent interaction of Eu^{2+} and O^{2-} prevented Eu^{2+} from showing red emission [13]. The above-mentioned previous studies had found that different activating ions and ligand sites affected the energy level distribution of the activated ions and f orbitals, thereby affecting the luminescence performance.

Doping with more than one lanthanide ion can make up for the deficiency of one lanthanide ion doping. For example, Li [14] successfully introduced $\text{Gd}^{3+}/\text{Er}^{3+}/\text{Lu}^{3+}$ into Bi_2Mo_6 to enhance its photocatalytic performance. Tang [15] introduced Ce^{3+} and Tb^{3+} into $\text{Na}_3\text{SrMg}_{11}(\text{PO}_4)_9$. There are relatively few reports on the lanthanide Eu^{2+} doped with $\text{M}_2\text{Si}_5\text{N}_8$ as the base material and further doped with another lanthanide. The study found that Tb^{3+} and Eu^{2+} co-doped $\text{Sr}_2\text{Si}_5\text{N}_8$ has a 20% increase in emission intensity [16]. Therefore, we want to systematically study the changes in the molecular structure and luminescence properties of Eu^{2+} and other Ln^{3+} co-doped systems. Among many lanthanides, the excitation spectrum of $\text{Pr}^{3+}4f-5d$ is relatively simple [8]. In the [Xe] (near nuclear pseudopotential electron) $4f_15d_1$ configuration during the excitation, Pr^{3+} has only one 4f energy level, which can occupy two different electrons. Tb's advantage is that in 4f-5d, the $4f_7[{}^8\text{S}_{7/2}]$ energy level is relatively stable, and the next higher $4f_7[{}^6\text{P}_1]5d_1$ energy level is about 3.5–4.0 eV higher. Therefore, it can be observed that $4f_8-4f_7({}^8\text{S}_{7/2})5d_1$ turns into an isolated state. Ce^{3+} is widely used as an activating ion in various fluorescent systems: $\text{Lu}_3\text{Al}_5\text{O}_{12}:\text{Ce}^{3+}$ [17], $\text{LaSi}_6\text{N}_{11}:\text{Ce}^{3+}$ [18], $\text{Tb}_3\text{Al}_5\text{O}_{12}:\text{Ce}^{3+}$ [19]. In summary, so we prefer to use any one of Ce^{3+} , Pr^{3+} , Tb^{3+} and Eu^{2+} doping for the $\text{Sr}_2\text{Si}_5\text{N}_8$ matrix to explore the changes in molecular structure and properties.

Li [20] used Ce^{3+} and Li^+ co-doping to replace two Sr^{2+} , among which Li^+ was used as a charge compensator for the charge imbalance caused by the partial replacement of Sr^{2+} by Ln^{3+} . Li^+ was widely used in phosphor doping such as $\text{CaLiAl}_3\text{N}_4$ [21], $\text{Sr}_4\text{LiAl}_{11}\text{N}_{14}$ [22], $\text{Li}_2\text{Ca}_2\text{Mg}_2\text{Si}_2\text{N}_6$ [23].

To realize the fundamental principal research on the luminescence characteristics, Fang [24] used the first principles to calculate the molecular structure and energy band structure of $\text{M}_2\text{Si}_5\text{N}_8$ ($\text{M} = \text{Ca}, \text{Sr}$). Shen [25] studied the band structure of $\text{Sr}_2\text{Si}_5\text{N}_8:\text{Eu}^{2+}$ through first-principles calculations and combined experiments to reveal the mechanism of luminescence. Density functional theory (DFT) based on first-principles ideas has been successfully applied to the study of microscopic particle systems. In this paper, combined with previous studies, first-principles calculations are used to study the model of Ce^{3+} , Pr^{3+} , Tb^{3+} , respectively, with Li^+ co-doped $\text{Sr}_2\text{Si}_5\text{N}_8$ matrix system and $\text{Ce}^{3+}/\text{Pr}^{3+}/\text{Tb}^{3+}$, respectively, with Eu^{2+} , Li^+ three types of ions co-doped $\text{Sr}_2\text{Si}_5\text{N}_8$ matrix. The optimized structural parameters of the co-doping model for different ion species and sites are presented. We calculate the energy band and density of states of varying doping systems to analyze the electronic structure.

2. Results and Discussion

2.1. Structures Distortion of Doped Models

In Table 1, a (Å), b (Å), c (Å) are the three sets of edge lengths of the unit cell. α , β , γ ($^\circ$) are, respectively, the angle between b and c ; a and c ; a and b . Polyhedral volume (Å^3) is the coordination polyhedron volume of Ln and N. Distortion index (Å) is the distance a ligand moves after the d/f orbital energy level splits and stabilizes, which reflects distortion effect. Distortion effect: For transition element/rare earth element ions with a high coordination number (>6), high-spin d/f orbitals and low-spin d/f orbitals are unstable in regular polyhedrons, which will cause these d/f orbits to undergo further splitting in energy, in order to stabilize the ion, causing the coordination relationship to deviate from the symmetry of the regular polyhedron. Effective coordination number means that due to the regular coordination polyhedron's structural distortion, the bond length between the ligand and the central atom changes, resulting in non-integer coordination.

Table 1. Cell parameters and [LnN] polyheral structures of $\text{Sr}_2\text{Si}_5\text{N}_8$ and $\text{Sr}_2\text{Si}_5\text{N}_8$ doped by Ln (Ce^{3+} , Pr^{3+} , Tb^{3+})/ Li^+ , Eu^{2+} .

$2 \times 2 \times 1$	Cell Parameters				Volume (Å^3)	[LnN] Polyhedral Volume (Å^3)	[LnN] Distortion Index (Å)	[LnN] Effective Coordination Number
Supercells	a (Å)	b (Å)	c (Å)	α, β, γ ($^\circ$)				
$\text{Sr}_2\text{Si}_5\text{N}_8(\text{Sr}_2)$	11.498	6.881	9.405	$\alpha = \beta = \gamma = 90.0$	744.074	48.866	0.062	6.707
$\text{Sr}_2\text{Si}_5\text{N}_8(\text{Sr}_1)$	11.498	6.881	9.405	$\alpha = \beta = \gamma = 90.0$	744.074	32.657	0.075	5.448
$\text{Eu}_{\text{Si}2}\text{-Sr}_2\text{Si}_5\text{N}_8$	11.498	6.876	9.403	$\alpha = 89.9,$ $\beta = \gamma = 90.0$	743.131	48.545	0.072	5.771
$\text{Eu}_{\text{Sr}1}\text{-Sr}_2\text{Si}_5\text{N}_8$	11.493	6.876	9.402	$\alpha = 90.1,$ $\beta = \gamma = 90.0$	743.046	32.379	0.090	4.728
$\text{Ce}_{\text{Sr}1}\text{Li}_{\text{Sr}1}\text{-Sr}_2\text{Si}_5\text{N}_8$	11.492	6.874	9.373	$\alpha = 90.4,$ $\beta = \gamma = 90.0$	740.450	27.921	0.119	4.919
$\text{Ce}_{\text{Sr}1}\text{Li}_{\text{Sr}2}\text{-Sr}_2\text{Si}_5\text{N}_8$	11.505	6.869	9.376	$\alpha = 90.1,$ $\beta = \gamma = 90$	741.010	27.857	0.110	4.776
$\text{Ce}_{\text{Sr}2}\text{Li}_{\text{Sr}1}\text{-Sr}_2\text{Si}_5\text{N}_8$	11.485	6.876	9.370	$\alpha = 89.9,$ $\beta = \gamma = 90$	739.910	45.191	0.092	5.550
$\text{Ce}_{\text{Sr}2}\text{Li}_{\text{Sr}2}\text{-Sr}_2\text{Si}_5\text{N}_8$	11.504	6.863	9.380	$\alpha = 89.7,$ $\beta = \gamma = 90$	740.700	44.354	0.090	5.597
$\text{Pr}_{\text{Sr}1}\text{Li}_{\text{Sr}1}\text{-Sr}_2\text{Si}_5\text{N}_8$	11.487	6.873	9.372	$\alpha = 90.4,$ $\beta = \gamma = 90$	739.830	27.797	0.123	4.849
$\text{Pr}_{\text{Sr}1}\text{Li}_{\text{Sr}2}\text{-Sr}_2\text{Si}_5\text{N}_8$	11.501	6.872	9.372	$\alpha = 90.1,$ $\beta = \gamma = 90.0$	740.680	27.689	0.114	4.645
$\text{Pr}_{\text{Sr}2}\text{Li}_{\text{Sr}1}\text{-Sr}_2\text{Si}_5\text{N}_8$	11.498	6.881	9.405	$\alpha = \beta = \gamma = 90.0$	739.340	45.213	0.101	5.420
$\text{Pr}_{\text{Sr}2}\text{Li}_{\text{Sr}2}\text{-Sr}_2\text{Si}_5\text{N}_8$	11.502	6.863	9.380	$\alpha = 89.7,$ $\beta = \gamma = 90.0$	740.450	44.345	0.093	5.337
$\text{Tb}_{\text{Sr}1}\text{Li}_{\text{Sr}1}\text{-Sr}_2\text{Si}_5\text{N}_8$	11.470	6.863	9.360	$\alpha = 90.5,$ $\beta = \gamma = 90.0$	736.970	27.321	0.154	4.676
$\text{Tb}_{\text{Sr}1}\text{Li}_{\text{Sr}2}\text{-Sr}_2\text{Si}_5\text{N}_8$	11.493	6.859	9.370	$\alpha = 90.1,$ $\beta = \gamma = 90.0$	738.970	27.300	0.147	4.496
$\text{Tb}_{\text{Sr}2}\text{Li}_{\text{Sr}1}\text{-Sr}_2\text{Si}_5\text{N}_8$	11.479	6.850	9.376	$\alpha = 89.9,$ $\beta = \gamma = 90.0$	737.230	44.902	0.150	4.724

The structure of $\text{Tb}_{\text{Sr}2}\text{Li}_{\text{Sr}2}\text{-Sr}_2\text{Si}_5\text{N}_8$ cannot converge after optimization. This model is unlikely to exist in the actual doping process, so subsequent calculations are not considered. The ionic radius of Sr^{2+} (1.18 Å), Eu^{2+} (1.17 Å), Ce^{3+} (1.02 Å), Pr^{3+} (0.99 Å), Tb^{3+} (0.92 Å), Li^+ (0.68 Å) [26] (regardless of the coordination number) decreases from left to right; Eu^{2+} , $\text{Ce}^{3+}/\text{Li}^+$, $\text{Pr}^{3+}/\text{Li}^+$ replace Sr^{2+} in turn. Due to the cationic ligand's volume coarctation, the lattice constant and unit cell volume will be slightly smaller. The volume of the doped system is smaller than that of undoped lanthanide ions. $\text{Sr}_2\text{Si}_5\text{N}_8$ volume, unit cell volume and doped ion radius are positively correlated. The average bond length between the lanthanide ion and N becomes shorter, making the bond between the lanthanide ion and the surrounding N stronger. The structure is more compact, the crystal field strength increases, and there will be a redshift tendency. Comparing the system in which the same lanthanide ion replaces eight-coordinate Sr^{2+} and ten-coordinate Sr^{2+} , we find that the distortion degree of eight-coordinate Sr^{2+} is greater than that of ten-coordinate Sr^{2+} . The formation of an eight-coordinate structure will produce a stronger electron cloud. The

nephelauxetic effect (NE) produces a centroid shift, which has a synergistic effect with the above redshift. However, for trivalent lanthanide ions doped with the same coordination number, the different Li^+ sites have almost no effect on the structure, which is only used to balance the charge.

Figure 1a shows the average bond length of $[\text{LnN}_8]$ and $[\text{LnN}_{10}]$, where AE represents the average bond length of $[\text{SrN}_8]$ and $[\text{SrN}_{10}]$ ligands in $\text{Sr}_2\text{Si}_5\text{N}_8$ primitive unit cells. It can be seen from the figure that the average bond length decreases with the decrease in the ion radius. $\text{Ln}_{\text{Sr}_2}\text{Li}_{\text{Sr}_1}\text{-Sr}_2\text{Si}_5\text{N}_8$ has the most extended bond length on average, and $\text{Ln}_{\text{Sr}_1}\text{Li}_{\text{Sr}_1}\text{-Sr}_2\text{Si}_5\text{N}_8$ is the shortest. Figure 1b is a schematic diagram of $\text{Ce}_{\text{Sr}_1}\text{Li}_{\text{Sr}_1}\text{-Sr}_2\text{Si}_5\text{N}_8$ $[\text{CeN}_{10}]$ and $\text{Eu}_{\text{Sr}_1}\text{-Sr}_2\text{Si}_5\text{N}_8$ $[\text{EuN}_{10}]$. Atoms (10 N) are selected from the 32 N atoms to form a ten-coordinate polyhedron in the figure.

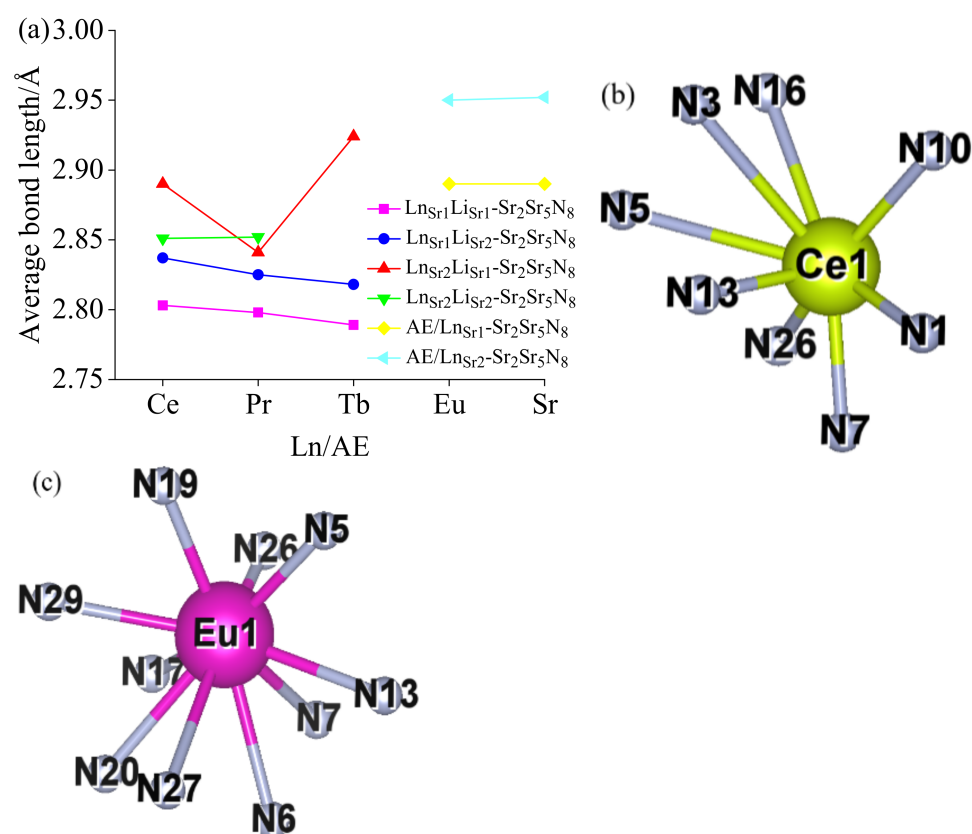


Figure 1. (a) Average bond length of $[\text{LnN}_8]$ and $[\text{LnN}_{10}]$. (b) Structure diagram of $[\text{CeN}_8]$. (c) Structure diagram of $[\text{EuN}_{10}]$.

2.1.1. Ln-Li Distance and $[\text{SrN}]$ Coordination Polyhedron Parameters of $\text{Sr}_2\text{Si}_5\text{N}_8:\text{Ln}^{3+}/\text{Li}^+$

Figures 2 and 3 describes the distance between Ln^{3+} and Li^+ . In the $\text{Sr}_2\text{Si}_5\text{N}_8$ matrix, the selected doping (Sr) site is the same distance as $\text{Sr}_1\text{-Sr}_1$ and $\text{Sr}_2\text{-Sr}_2$, before being replaced by $\text{Ln}^{3+}/\text{Li}^+$, which has a distance of 5.748 Å; the distance is 3.467 Å between $\text{Sr}_1\text{-Sr}_2$. When Ln^{3+} and Li^+ are doped to replace Sr_1 , in the order of Pr^{3+} , Ce^{3+} , Tb^{3+} , the Ln-Li distances increased by 0.06 Å, 0.066 Å, 0.037 Å, respectively, and the degree of distortion was 1.05%, 1.14% and 0.64%. The overall deviation is not significant. When Ln^{3+}/Li replaces different sites, the degree of distortion is always above 7.56%. From the perspective of the degree of lattice distortion, it is unlikely to occur in actual situations. When $\text{Ln}^{3+}/\text{Li}^+$ is doped to replace Sr_2 , the distortion degree of $\text{Pr}_{\text{Sr}_2}\text{Li}_{\text{Sr}_2}\text{-Sr}_2\text{Si}_5\text{N}_8$ and $\text{Ce}_{\text{Sr}_2}\text{Li}_{\text{Sr}_2}\text{-Sr}_2\text{Si}_5\text{N}_8$ is about 2.40%. After $\text{Ln}_{\text{Sr}_1}\text{Li}_{\text{Sr}_1}\text{-Sr}_2\text{Si}_5\text{N}_8$ and $\text{Ln}_{\text{Sr}_2}\text{Li}_{\text{Sr}_2}\text{-Sr}_2\text{Si}_5\text{N}_8$ are doped to replace the Sr site, the distance between Ln-Li becomes longer, while $\text{Ln}_{\text{Sr}_1}\text{Li}_{\text{Sr}_2}$ and $\text{Ln}_{\text{Sr}_2}\text{Li}_{\text{Sr}_1}$ have shorter distances than that before doping.

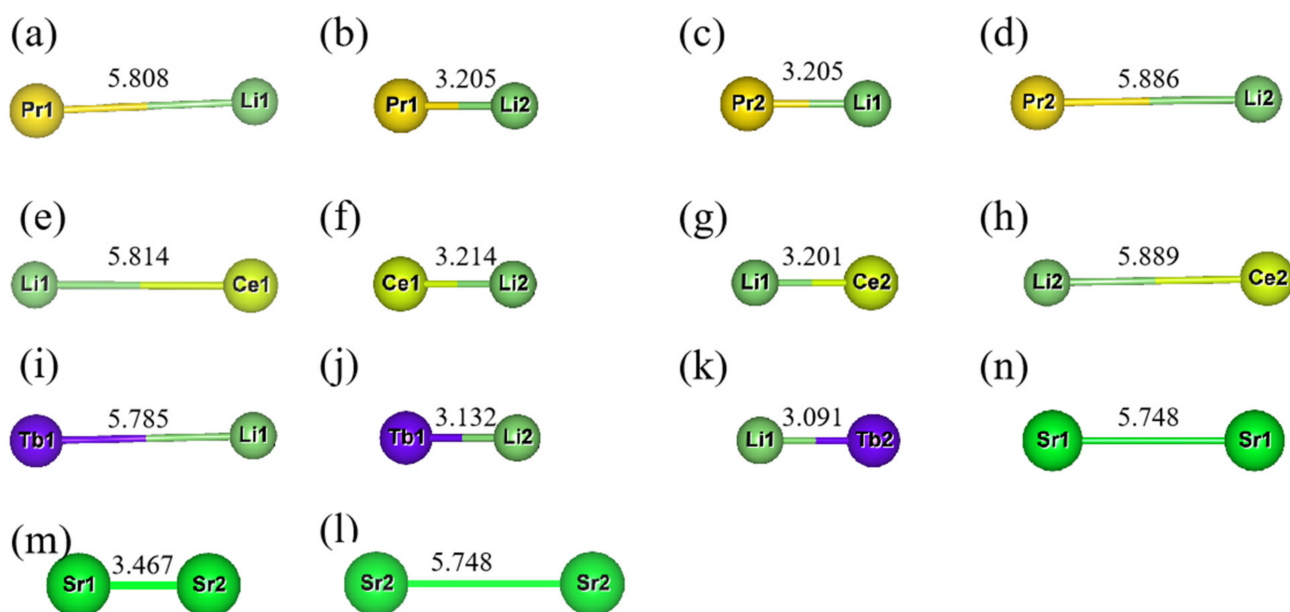


Figure 2. The distance change after Ln^{3+} and Li^+ replace Sr_1 and Sr_2 in doped $\text{Sr}_2\text{Si}_5\text{N}_8$ (a–k) $\text{Pr}_{\text{Sr}_1}\text{Li}_{\text{Sr}_1}\text{-Sr}_2\text{Si}_5\text{N}_8$, $\text{Pr}_{\text{Sr}_1}\text{Li}_{\text{Sr}_2}\text{-Sr}_2\text{Si}_5\text{N}_8$, $\text{Pr}_{\text{Sr}_2}\text{Li}_{\text{Sr}_1}\text{-Sr}_2\text{Si}_5\text{N}_8$, $\text{Pr}_{\text{Sr}_2}\text{Li}_{\text{Sr}_2}\text{-Sr}_2\text{Si}_5\text{N}_8$, $\text{Ce}_{\text{Sr}_1}\text{Li}_{\text{Sr}_1}\text{-Sr}_2\text{Si}_5\text{N}_8$, $\text{Ce}_{\text{Sr}_1}\text{Li}_{\text{Sr}_2}\text{-Sr}_2\text{Si}_5\text{N}_8$, $\text{Ce}_{\text{Sr}_2}\text{Li}_{\text{Sr}_1}\text{-Sr}_2\text{Si}_5\text{N}_8$, $\text{Ce}_{\text{Sr}_2}\text{Li}_{\text{Sr}_2}\text{-Sr}_2\text{Si}_5\text{N}_8$, $\text{Tb}_{\text{Sr}_1}\text{Li}_{\text{Sr}_1}\text{-Sr}_2\text{Si}_5\text{N}_8$, $\text{Tb}_{\text{Sr}_1}\text{Li}_{\text{Sr}_2}\text{-Sr}_2\text{Si}_5\text{N}_8$, $\text{Tb}_{\text{Sr}_2}\text{Li}_{\text{Sr}_1}\text{-Sr}_2\text{Si}_5\text{N}_8$; (n–l) is the Sr–Sr distance before doping.

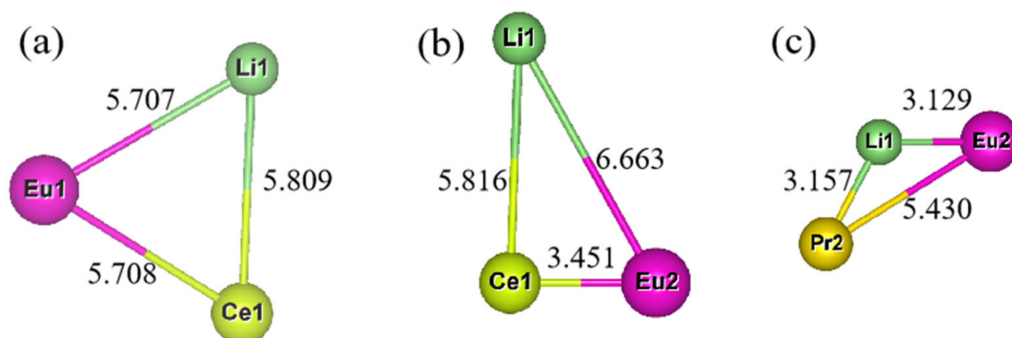


Figure 3. (a–c): Ln–Li, Eu–Li, Eu–Ln's distance diagram after $\text{Eu}_{\text{Sr}_1}\text{Ce}_{\text{Sr}_1}\text{Li}_{\text{Sr}_1}\text{-Sr}_2\text{Si}_5\text{N}_8$, $\text{Eu}_{\text{Sr}_2}\text{Ce}_{\text{Sr}_1}\text{Li}_{\text{Sr}_1}\text{-Sr}_2\text{Si}_5\text{N}_8$, $\text{Eu}_{\text{Sr}_2}\text{Pr}_{\text{Sr}_2}\text{Li}_{\text{Sr}_1}\text{-Sr}_2\text{Si}_5\text{N}_8$ doped with $\text{Sr}_2\text{Si}_5\text{N}_8$ matrix.

Table 2 is the detailed description of Figure 4. In Table 2, we can see that when Ln doping replaces the site, $[\text{SrN}_{10}]$ tends to appear with two coordination types, one has an effective coordination number greater than 6.707 \AA , and the other is less than 6.707 \AA (6.707 \AA is undoped $[\text{SrN}_{10}]$ effective coordination number). The effective coordination number of $[\text{SrN}_{10}]$ increases, while the effective coordination number of $[\text{SrN}_8]$ decreases. When Ln^{3+} doping replaces the Sr_2 site, it is similar to Ln^{3+} substitution doping of the Sr_1 site. $[\text{SrN}_8]$ tends to have two effective coordination numbers: the effective coordination number of $[\text{SrN}_8]$ increased, and the effective coordination number of $[\text{SrN}_{10}]$ decreased. The above phenomenon showed that after the structure optimization of Ln doping to replace Sr sites, the effective coordination number of $[\text{SrN}]$ in other Sr sites is reduced with the same coordination number as doping to replace Sr is reduced. Combining with three factors: $[\text{LnN}]$ coordination polyhedron structure, Ln–Li distance and $[\text{SrN}]$ coordination polyhedron structure, the $\text{Ln}_{\text{Sr}_1}\text{Li}_{\text{Sr}_1}\text{-Sr}_2\text{Si}_5\text{N}_8$ doped-model can exist reasonably.

Table 2. [SrN] Coordination polyhedron parameters of Sr₂Si₅N₈ doped by Ln (Ce³⁺, Pr³⁺, Tb³⁺)/Li⁺.

$2 \times 2 \times 1$ Supercell	[SrN] Average Bond Length (Å)	[SrN] Polyhedral Volume (Å ³)	[SrN] Distortion Index (Å)	[SrN] Effective Coordination Number	[SrN] Coordination Number
Ce _{Sr1} Li _{Sr1} -Sr ₂ Si ₅ N ₈	2.994	49.700	0.0723	7.000	10
	2.942	48.317	0.0720	6.620	10
	2.886	32.405	0.0757	5.420	8
Ce _{Sr1} Li _{Sr2} -Sr ₂ Si ₅ N ₈	2.925	47.655	0.063	7.070	10
	2.954	48.845	0.073	6.358	10
	2.907	35.144	0.086	5.052	8
Ce _{Sr2} Li _{Sr1} -Sr ₂ Si ₅ N ₈	2.956	49.440	0.066	6.211	10
	2.963	45.359	0.088	5.889	10
	2.879	32.349	0.081	5.741	8
Ce _{Sr2} Li _{Sr2} -Sr ₂ Si ₅ N ₈	2.975	49.291	0.075	5.989	10
	2.870	34.093	0.080	5.350	8
	2.909	33.711	0.067	5.899	8
Pr _{Sr1} Li _{Sr1} -Sr ₂ Si ₅ N ₈	2.940	48.289	0.072	6.646	10
	2.994	49.734	0.073	7.022	10
	2.884	32.335	0.076	5.434	8
Pr _{Sr1} Li _{Sr2} -Sr ₂ Si ₅ N ₈	2.923	47.601	0.062	7.148	10
	2.956	48.950	0.072	6.378	10
	2.907	35.144	0.085	5.085	8
Pr _{Sr2} Li _{Sr1} -Sr ₂ Si ₅ N ₈	2.923	47.601	0.062	7.148	10
	2.907	35.144	0.085	5.085	8
	2.955	48.950	0.072	6.378	10
Pr _{Sr2} Li _{Sr2} -Sr ₂ Si ₅ N ₈	2.970	49.192	0.073	6.087	10
	2.872	34.160	0.081	5.321	8
	2.908	33.695	0.068	5.886	8
Tb _{Sr1} Li _{Sr1} -Sr ₂ Si ₅ N ₈	2.937	48.233	0.071	6.874	10
	2.999	49.821	0.075	6.968	10
	2.877	32.096	0.075	5.467	8
Tb _{Sr1} Li _{Sr2} -Sr ₂ Si ₅ N ₈	2.923	47.602	0.061	7.231	10
	2.963	49.304	0.073	6.116	10
	2.899	34.905	0.083	5.159	8
Tb _{Sr2} Li _{Sr1} -Sr ₂ Si ₅ N ₈	2.883	32.733	0.086	5.729	8
	2.958	49.914	0.079	5.940	10
	2.955	45.191	0.085	6.112	10
Eu _{Sr1} -Sr ₂ Si ₅ N ₈	2.947	48.690	0.061	6.735	10
	2.952	48.914	0.060	6.962	10
	2.888	32.658	0.074	5.449	8
Eu _{Sr2} -Sr ₂ Si ₅ N ₈	2.951	48.904	0.061	6.701	10
	2.888	32.706	0.072	5.625	8
	2.889	32.641	0.074	5.453	8
	2.942	38.657	0.085	5.536	8

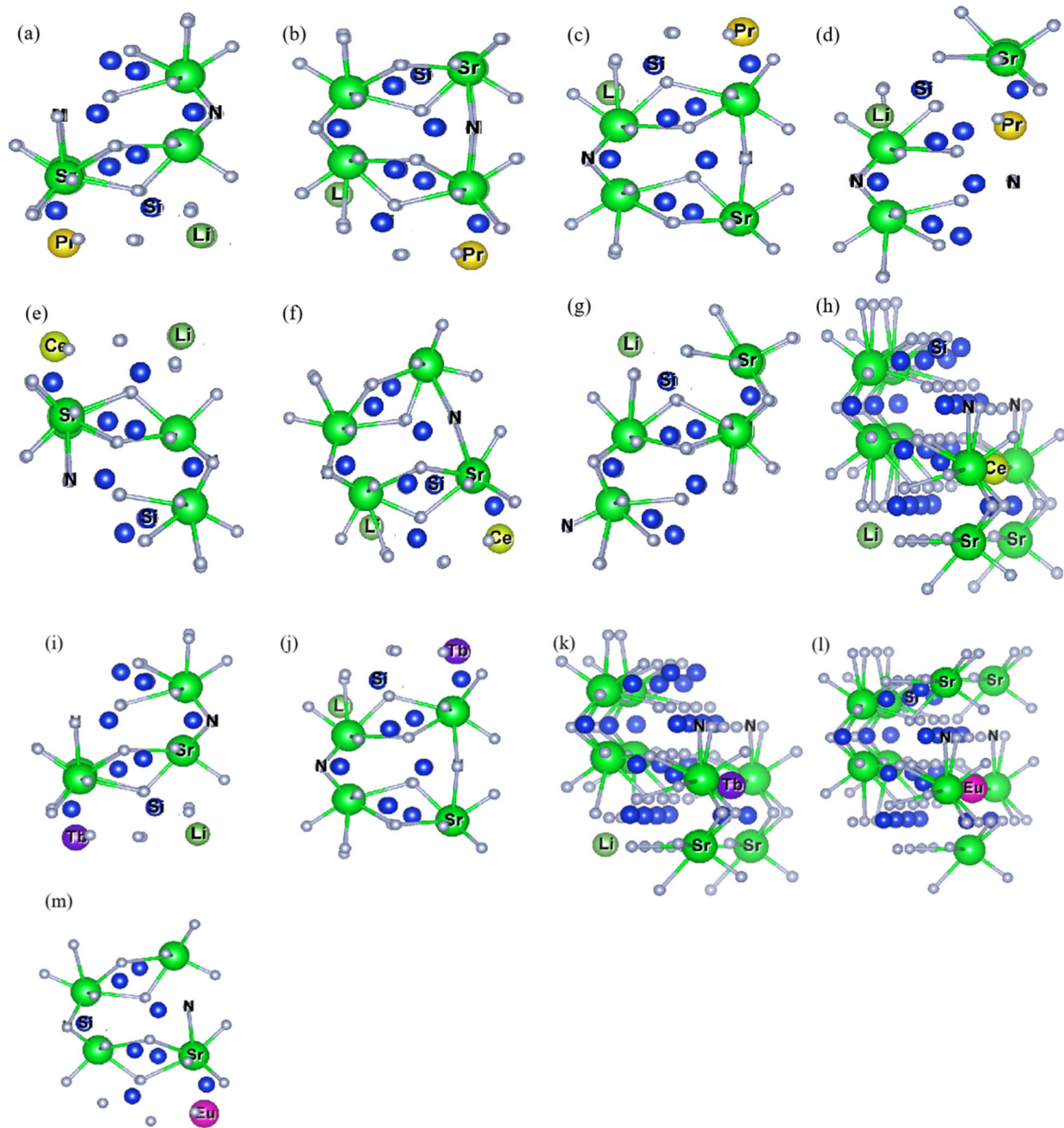


Figure 4. [SrN] coordination polyhedron diagram after substitution of $\text{Ln}^{3+}/\text{Li}^{+}$ for Sr_1 and Sr_2 sites in $\text{Sr}_2\text{Si}_5\text{N}_8$ (a–m) $\text{Pr}_{\text{Sr}_1}\text{Li}_{\text{Sr}_2}\text{-Sr}_2\text{Si}_5\text{N}_8$, $\text{Pr}_{\text{Sr}_1}\text{Li}_{\text{Sr}_2}\text{-Sr}_2\text{Si}_5\text{N}_8$, $\text{Pr}_{\text{Sr}_2}\text{Li}_{\text{Sr}_1}\text{-Sr}_2\text{Si}_5\text{N}_8$, $\text{Pr}_{\text{Sr}_2}\text{Li}_{\text{Sr}_2}\text{-Sr}_2\text{Si}_5\text{N}_8$, $\text{Ce}_{\text{Sr}_1}\text{Li}_{\text{Sr}_1}\text{-Sr}_2\text{Si}_5\text{N}_8$, $\text{Ce}_{\text{Sr}_1}\text{Li}_{\text{Sr}_2}\text{-Sr}_2\text{Si}_5\text{N}_8$, $\text{Ce}_{\text{Sr}_2}\text{Li}_{\text{Sr}_1}\text{-Sr}_2\text{Si}_5\text{N}_8$, $\text{Ce}_{\text{Sr}_2}\text{Li}_{\text{Sr}_2}$, $\text{Tb}_{\text{Sr}_1}\text{Li}_{\text{Sr}_1}\text{-Sr}_2\text{Si}_5\text{N}_8$, $\text{Tb}_{\text{Sr}_1}\text{Li}_{\text{Sr}_2}\text{-Sr}_2\text{Si}_5\text{N}_8$, $\text{Tb}_{\text{Sr}_2}\text{Li}_{\text{Sr}_1}\text{-Sr}_2\text{Si}_5\text{N}_8$, $\text{Eu}_{\text{Sr}_1}\text{-Sr}_2\text{Si}_5\text{N}_8$, $\text{Eu}_{\text{Sr}_2}\text{-Sr}_2\text{Si}_5\text{N}_8$.

2.1.2. Lattice Constant and [LnN] Ligand Parameters of $\text{Sr}_2\text{Si}_5\text{N}_8:\text{Ln}^{3+}/\text{Li}^{+}/\text{Eu}^{2+}$

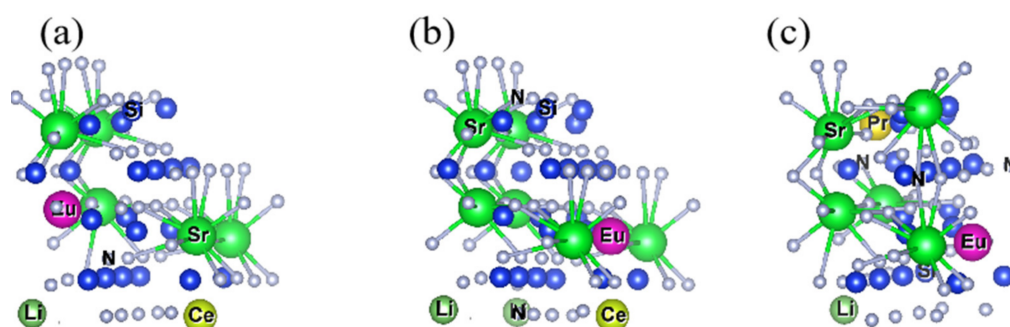
In Table 3, $\text{Ln}^{3+}/\text{Eu}^{2+}$ is the coordination polyhedron information of the ion and N. Except for the six ligand structures with three double lanthanide ions substituted for the Sr site, the other structures are not below the theoretical values. Only the following three doping models are Eu^{2+} and Ce^{3+} to replace Sr_1 , Eu^{2+} to replace Sr_2 , and Ce^{3+} to replace Sr_1 , Eu^{2+} replaces Sr_2 , Pr^{3+} replaces Sr_2 in line with the actual structure. Neither Tb^{3+} nor Eu^{2+} co-doped systems are desirable. The unit cell volume and ligand structure of the co-doped system did not change significantly from the single-doped system.

Table 3. Cell parameters and [LnN] polyhedral structures of Sr₂Si₅N₈ co-doped Eu²⁺/Ce³⁺/Li⁺ and Eu²⁺/Pr³⁺/Li⁺.

2 × 2 × 1 Supercells	Cell Parameters				Volume (Å ³)	[LnN] Polyhedral Volume (Å ³)	[LnN] Distortion Index (Å)	[LnN] Effective Coordination Number
	a (Å)	b (Å)	c (Å)	α,β,γ (°)				
Eu _{Sr1} Ce _{Sr1} Li _{Sr2} -Sr ₂ Si ₅ N ₈ (Eu)	11.490	6.874	9.375	α = 90.3, β = γ = 90.0	740.470	32.042	0.0947	4.654
Eu _{Sr1} Ce _{Sr1} Li _{Sr2} -Sr ₂ Si ₅ N ₈ (Ce)	11.490	6.874	9.375	α = 90.3, β = γ = 90.0	740.470	28.112	0.1219	4.926
Eu _{Sr2} Ce _{Sr1} Li _{Sr2} -Sr ₂ Si ₅ N ₈ (Eu)	11.492	6.867	9.370	α = 90.3, β = γ = 90.0	739.470	48.094	0.0613	6.455
Eu _{Sr2} Ce _{Sr1} Li _{Sr2} -Sr ₂ Si ₅ N ₈ (Ce)	11.492	6.867	9.370	α = 90.3, β = γ = 90.0	739.470	28.046	0.1254	5.026
Eu _{Sr2} Pr _{Sr2} Li _{Sr2} -Sr ₂ Si ₅ N ₈ (Eu)	11.480	6.8607	9.377	α = 90.3, β = γ = 90.0	738.566	48.574	0.0943	5.849
Eu _{Sr2} Pr _{Sr2} Li _{Sr2} -Sr ₂ Si ₅ N ₈ (Pr)	11.480	6.8607	9.377	α = 90.3, β = γ = 90.0	738.566	45.876	0.0880	4.752

2.1.3. Ln-Li-Eu distance and [SrN] Coordination Polyhedron Parameters of Sr₂Si₅N₈:Ln³⁺/Li⁺/Eu²⁺

After screening more than 30 models, a total of three models may exist stably after structure optimization. According to the order of Figure 4a–c, the distances before optimization of Ln-Li, Ln-Eu and Eu-Li are 5.748 Å, 5.748 Å, 5.748 Å; 5.748 Å, 3.467 Å, 6.713 Å; 3.467 Å, 5.748 Å, 3.467 Å. Among them, the distance between (a) and (b) does not change obviously before and after convergence, which is less than 0.1% compared with the original Sr-Sr distance. In summary, Combining Figure 5 and Table 4, we can draw the following conclusions: Eu_{Sr1}Ce_{Sr1}Li_{Sr1} and Eu_{Sr2}Ce_{Sr1}Li_{Sr1} can exist stably after Eu²⁺/Ce³⁺/Li⁺ co-doped with Sr₂Si₅N₈, without considering the formation energy conditions. In the Eu_{Sr2}Pr_{Sr2}Li_{Sr1}-model, there are three distance types: Ln-Eu, Ln-Li, and Eu-Li. Compared with the original Sr sites, the distance changes are 5.6%, 8.9%, and 9.7%, respectively. In the Eu²⁺/Tb³⁺/Li⁺-Sr₂Si₅N₈ model, the ionic radius of Tb³⁺ is too small, resulting in excessive structural distortion and difficulty in optimization convergence, so its structure cannot exist stably.

**Figure 5.** (a–c): [SrN] Coordination Polyhedron Diagram after Eu_{Sr1}Ce_{Sr1}Li_{Sr1}-Sr₂Si₅N₈, Eu_{Sr2}Ce_{Sr1}Li_{Sr1}-Sr₂Si₅N₈, Eu_{Sr2}Pr_{Sr2}Li_{Sr1}-Sr₂Si₅N₈ doped with Sr₂Si₅N₈ matrix.

2.2. Formation Energy of Doped Models

Figure 6 is the formation energy diagram of Ce³⁺ (Tb³⁺, Pr³⁺)/Li⁺ co-doped Sr₂Si₅N₈ with eight-coordinate (Sr₁) and ten-coordinate (Sr₂). From the definition of formation energy, the lower formation energy value means the target product is easier to form. Among all the values, Ce³⁺ and Li⁺'s formation energy co-doped in eight-coordinate and ten-coordinate systems, respectively, is the lowest. Pr³⁺ and Li⁺ co-doped together to replace eight-coordinate Sr has the highest formation energy. For Ce³⁺ and Tb³⁺, Ce³⁺ (Tb³⁺) and Li⁺ are, respectively, doped at the same Sr site to form lower energy. Pr and Li co-doped to replace ten-coordinate Sr²⁺ has the lower formation energy, and for co-doped

to replace eight-coordinate Sr^{2+} , the formation energy is the highest. Three kinds of lanthanide ions doping to replace Sr_2 are easier to generate in theory. The formation energy of Li^+ is lower when it is at the Sr_2 site, so the fixed Li^+ doping replaces Sr_2^{2+} . Ce^{3+} (Tb^{3+} , Pr^{3+})/ Li^+ / Eu^{2+} co-doped Sr_1 and Sr_2 of $\text{Sr}_2\text{Si}_5\text{N}_8$, in which Li^+ is fixedly doped instead of Sr_1^{2+} . $\text{Eu}_{\text{Sr}_1}\text{Ce}_{\text{Sr}_1}\text{Li}_{\text{Sr}_1}\text{-Sr}_2\text{Si}_5\text{N}_8$, $\text{Eu}_{\text{Sr}_2}\text{Ce}_{\text{Sr}_1}\text{Li}_{\text{Sr}_1}\text{-Sr}_2\text{Si}_5\text{N}_8$ and $\text{Eu}_{\text{Sr}_2}\text{Pr}_{\text{Sr}_2}\text{Li}_{\text{Sr}_1}\text{-Sr}_2\text{Si}_5\text{N}_8$'s formation energy levels are -1.2 eV, -5.2 eV, -5.18 eV. Compared with $\text{Eu}_{\text{Sr}_2}\text{Pr}_{\text{Sr}_2}\text{Li}_{\text{Sr}_1}\text{-Sr}_2\text{Si}_5\text{N}_8$, $\text{Sr}_2\text{Si}_5\text{N}_8\text{:Pr}^{3+}/\text{Li}^+$ has a lower formation energy at around -2.8 eV. The formation energy of $\text{Sr}_2\text{Si}_5\text{N}_8\text{:Ce}^{3+}/\text{Li}^+/\text{Eu}^{2+}$ is 1.2 eV lower than $\text{Sr}_2\text{Si}_5\text{N}_8\text{:Ce}^{3+}/\text{Li}^+$, so $\text{Eu}_{\text{Sr}_1}\text{Ce}_{\text{Sr}_1}\text{Li}_{\text{Sr}_1}\text{-Sr}_2\text{Si}_5\text{N}_8$, $\text{Eu}_{\text{Sr}_2}\text{Ce}_{\text{Sr}_1}\text{Li}_{\text{Sr}_1}\text{-Sr}_2\text{Si}_5\text{N}_8$ could exist in theory.

Table 4. [SrN] Coordination polyhedron parameters of $\text{Sr}_2\text{Si}_5\text{N}_8$ doped by Ln (Ce^{3+} , Pr^{3+} , Tb^{3+})/ $\text{Li}^+/\text{Eu}^{2+}$.

$2 \times 2 \times 1$ Supercell	[SrN] Average Bond Length (Å)	[SrN] Polyhedral Volume (Å ³)	[SrN] Distortion Index (Å)	[SrN] Effective Coordination Number	[SrN] Coordination Number
$\text{Eu}_{\text{Sr}_1}\text{Ce}_{\text{Sr}_1}\text{Li}_{\text{Sr}_1}$	2.941	48.361	0.0666	6.884	10
	2.989	49.546	0.0721	7.040	10
	2.887	32.507	0.0755	5.406	8
$\text{Eu}_{\text{Sr}_2}\text{Ce}_{\text{Sr}_1}\text{Li}_{\text{Sr}_1}$	2.945	48.444	0.0718	6.590	10
	2.991	49.691	0.0705	7.039	10
	2.880	32.241	0.0755	5.427	8
$\text{Eu}_{\text{Sr}_2}\text{Pr}_{\text{Sr}_2}\text{Li}_{\text{Sr}_1}$	2.960	49.248	0.0646	6.260	10
	2.863	31.895	0.0825	5.680	8
	2.889	32.623	0.0753	5.360	8

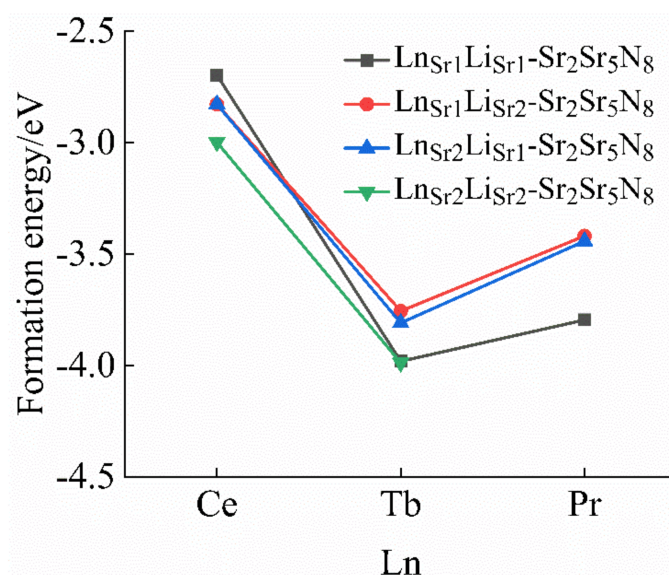


Figure 6. Formation energies of $\text{Ln}^{3+}/\text{Li}^+$ elements co-doped $\text{Sr}_2\text{Si}_5\text{N}_8$.

2.3. Band Structures and Density of States

We first calculated the ground state energy band and state density of Eu^{2+} single-doped $\text{Sr}_2\text{Si}_5\text{N}_8$ and Tb^{3+} (Ce^{3+} , Pr^{3+})/ Li^+ co-doped $\text{Sr}_2\text{Si}_5\text{N}_8$ systems, as shown in Figure 7, for our subsequent calculations of $\text{Eu}^{2+}/\text{Ce}^{3+}$ (Tb^{3+} , Pr^{3+})/ Li^+ ion co-doping, which provides a basis for comparison. The calculated bandgap of $\text{Sr}_2\text{Si}_5\text{N}_8\text{:Eu}^{2+}$ is 3.21 eV, which is slightly smaller than the experimental bandgap because the approximate processing of the DFT exchange-correlation term causes the bandgap to become narrower [27]. In the (a–l) ground-

state band structure diagram, their direct bandgaps are $\text{Ce}_{\text{Sr}1}\text{Li}_{\text{Sr}1}\text{-Sr}_2\text{Si}_5\text{N}_8$: 3.03 eV, $\text{Ce}_{\text{Sr}1}\text{Li}_{\text{Sr}2}\text{-Sr}_2\text{Si}_5\text{N}_8$: 3.15 eV, $\text{Ce}_{\text{Sr}2}\text{Li}_{\text{Sr}1}\text{-Sr}_2\text{Si}_5\text{N}_8$: $\text{Ce}_{\text{Sr}2}\text{Li}_{\text{Sr}1}\text{-Sr}_2\text{Si}_5\text{N}_8$: $\text{Sr}_2\text{Si}_5\text{N}_8$: 3.09 eV, $\text{Pr}_{\text{Sr}1}\text{Li}_{\text{Sr}1}\text{-Sr}_2\text{Si}_5\text{N}_8$: 2.97 eV, $\text{Pr}_{\text{Sr}1}\text{Li}_{\text{Sr}2}\text{-Sr}_2\text{Si}_5\text{N}_8$: 3.27 eV, $\text{Pr}_{\text{Sr}2}\text{Li}_{\text{Sr}1}\text{-Sr}_2\text{Si}_5\text{N}_8$: 3.27 eV, $\text{Pr}_{\text{Sr}2}\text{Li}_{\text{Sr}2}\text{-Sr}_2\text{Si}_5\text{N}_8$: 3.30 eV, $\text{Tb}_{\text{Sr}1}\text{Li}_{\text{Sr}1}\text{-Sr}_2\text{Si}_5\text{N}_8$: 3.30 eV, $\text{Tb}_{\text{Sr}1}\text{Li}_{\text{Sr}2}\text{-Sr}_2\text{Si}_5\text{N}_8$: 3.27 eV, $\text{Tb}_{\text{Sr}1}\text{Li}_{\text{Sr}2}\text{-Sr}_2\text{Si}_5\text{N}_8$: 3.24 eV. The high symmetry point G (reciprocal space), has the lowest energy at conduction band minimum (CBM), while some high symmetry points (Z) have the lowest CBM, and the highest valence band maximum (VBM). The lowest point of energy is between Z and G (Figure S1, Supporting Information). Due to the large energy gap between VBM and CBM (0.3 eV), the transition from VBM to CBM is an indirect bandgap transition. The direct bandgaps of (a–k) are 0.51 eV, 0.78 eV, 0.87 eV, 0.57 eV; 0.39 eV, 0.18 eV, 0.18 eV, 0.27 eV, 1.98 eV, 2.07 eV, 2.01 eV (Figure S1, Supporting Information); (a–k)'s indirect bandgaps are 3.03 eV, 3.15 eV, 3.24 eV, 3.09 eV, 2.97 eV, 3.27 eV, 3.27 eV, 3.30 eV, 3.30 eV, 3.27 eV, 3.24 eV. We compare four data from each of the same lanthanide elements. Excluding $\text{Pr}_{\text{Sr}2}\text{Li}_{\text{Sr}2}\text{-Sr}_2\text{Si}_5\text{N}_8$, the bandgap is 3.30 eV, and the other five $\text{Ln}_n\text{Li}_n\text{-Sr}_2\text{Si}_5\text{N}_8$ are all about 3 eV. Except for $\text{Pr}_{\text{Sr}2}\text{Li}_{\text{Sr}2}\text{-Sr}_2\text{Si}_5\text{N}_8$, (f–h)'s 4f is closed to the CBM, the 4f energy levels of the ground-state lanthanide ions are distributed near the Fermi level (set VBM to 0), which is the premise of the lanthanide ion itself as the luminescence center. (a) $\text{Ce}_{\text{Sr}1}\text{Li}_{\text{Sr}1}\text{-Sr}_2\text{Si}_5\text{N}_8$ and (e) $\text{Pr}_{\text{Sr}1}\text{Li}_{\text{Sr}1}\text{-Sr}_2\text{Si}_5\text{N}_8$ have the smallest band gaps in their respective doping models, indicating that these two doping models have a high peak in the excited state and better luminous performance.

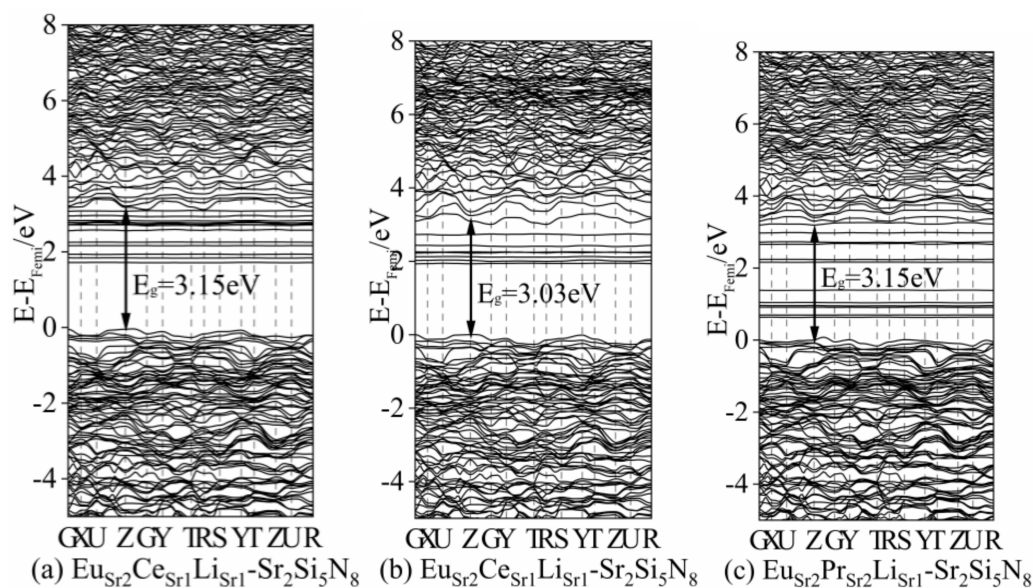


Figure 7. Band structures of doped structures: (a) $\text{Eu}_{\text{Sr}2}\text{Ce}_{\text{Sr}1}\text{Li}_{\text{Sr}1}\text{-Sr}_2\text{Si}_5\text{N}_8$; (b) $\text{Eu}_{\text{Sr}2}\text{Ce}_{\text{Sr}1}\text{Li}_{\text{Sr}1}\text{-Sr}_2\text{Si}_5\text{N}_8$; (c) $\text{Pr}_{\text{Sr}2}\text{Eu}_{\text{Sr}2}\text{Li}_{\text{Sr}1}\text{-Sr}_2\text{Si}_5\text{N}_8$.

The states diagram's density shows that the main components of VBM are 2p of N, 3s, 3p of Si, and CBM is mainly composed of 4f energy level of La, 5d, 5s orbitals of Sr and 3p, 3s of Si. Eu 6s, Eu 5p, Ce 6s, Ce 5p, Pr 6s, Pr 5p, Tb 6s and Tb 5p are minor in their contributions. The (Partial Density of State, PDOS) of Ce, Sr, N, Si in $\text{Ce}_{\text{Sr}1}\text{Li}_{\text{Sr}1}\text{-Sr}_2\text{Si}_5\text{N}_8$ are the same as the four PDOS in Sikander Azam's calculation about $\text{Sr}_2\text{Si}_5\text{N}_8\text{:Ce}^{3+}$ [28]. Figure 7a has strong peaks at 2.04 eV and 2.46 eV, Figure S1b has approximately the same values at 2.07 eV, 2.10 eV, 2.25 eV, and 2.34 eV, while Figure S1c has a higher peak at 2.31 eV. Figure S1d has peaks of similar intensity at 2.25 eV, 2.43 eV, and 2.49 eV. The 4f energy level of Figure S1f–h is between 2.28 and 2.52 eV, and the 4f peak value of Pr^{3+} in Figure S1e is very high. If Pr^{3+} is the luminous center, the luminous intensity is much higher than Figure S1f–h. The 4f of Tb^{3+} in Figure S1j has a higher peak intensity at 1.17 eV, which has a good potential for activating ions.

Figure 7 shows the energy bands and state density of the three kinds of triple-doped ions systems, $\text{Eu}_{\text{Sr}1}\text{Ce}_{\text{Sr}1}\text{Li}_{\text{Sr}2}\text{-Sr}_2\text{Si}_5\text{N}_8$, $\text{Eu}_{\text{Sr}2}\text{Ce}_{\text{Sr}1}\text{Li}_{\text{Sr}2}\text{-Sr}_2\text{Si}_5\text{N}_8$, $\text{Pr}_{\text{Sr}2}\text{Eu}_{\text{Sr}2}\text{Li}_{\text{Sr}2}\text{-Sr}_2\text{Si}_5\text{N}_8$. In $\text{Eu}_{\text{Sr}1}\text{Ce}_{\text{Sr}1}\text{Li}_{\text{Sr}2}\text{-Sr}_2\text{Si}_5\text{N}_8$, Eu^{2+} is the main component in the forbidden band. Ce^{3+} is close to the bottom of the conduction band. $\text{Eu}_{\text{Sr}2}\text{Ce}_{\text{Sr}1}\text{Li}_{\text{Sr}2}\text{-Sr}_2\text{Si}_5\text{N}_8$ is in the conduction band and has low intensity. Therefore, among the lanthanide ions of this system, only Ce^{3+} is the luminescence center. For $\text{Pr}_{\text{Sr}2}\text{Eu}_{\text{Sr}2}\text{Li}_{\text{Sr}2}\text{-Sr}_2\text{Si}_5\text{N}_8$, the band distribution is relatively dense. The 5d electrons in the excited state may produce multi-level transitions [29].

Determination of DFT+U Parameters of Each System

In Table 5, as the value of U_{eff} increases from 0 to 8 eV, when Eu^{2+} is equal to 6 eV, the 4f electron orbital of Eu^{2+} appears at the top of the valence band. When $U_{\text{eff}} = 8$ eV, the filled state 4f orbital has wholly entered the valence band, and the energy level is about -1 eV (set the top of the valence band as the Fermi level, that is, $E_f = 0$ eV). When $U_{\text{eff}} = 4$ eV, $\text{Sr}_2\text{Si}_5\text{N}_8:\text{Eu}_{\text{Sr}1}^{2+}$ and $\text{Sr}_2\text{Si}_5\text{N}_8:\text{Eu}_{\text{Sr}2}^{2+}$'s 4f-CBM energy difference is 2.22 eV and 2.23 eV, respectively, according to the energy wavelength conversion formula:

$$E = \frac{hc}{\lambda} \quad (1)$$

In the above formula, E (energy)—eV, h (Planck's constant) = 6.63×10^{-34} J·s, $k = 1.6 \times 10^{-19}$ J/eV, C (speed of light) = 3×10^{17} nm/s, λ (wavelength)—nm. The parameters can be obtained in the following formula:

$$\lambda = \frac{1240}{E} \quad (2)$$

The direct bandgaps of Figure 8a–c are 0.51 eV, 0.78 eV, 0.87 eV, 0.57 eV; 0.39 eV, 0.18 eV, 0.18 eV, 0.27 eV; 1.98 eV, 2.07 eV, 2.01 eV, respectively. The U_{eff} value makes 4f-CBM fall in the appropriate energy range, the U_{eff} introduced by (a–k) are: 5 eV, 5 eV, 5 eV, 6 eV; 4 eV, 6 eV, 6 eV, 6 eV; 2 eV, 2 eV, 2 eV, 2 eV. The energy difference of 4f-CBM in (a–k) with different U_{eff} is: 2.42 eV, 2.53 eV, 2.62 eV, 2.68 eV, 1.79 eV, 2.28 eV, 2.28 eV, 2.37 eV; 2.69 eV, 2.76 eV, 2.73 eV.

Table 5. Energy level difference of Eu 4f-CBM of $\text{Sr}_2\text{Si}_5\text{N}_8:\text{Eu}^{2+}$ with different U_{eff} parameters.

U_{eff} (eV)	Eu^{2+} 4f-CBM(eV)	
	Eu_1^{2+}	Eu_2^{2+}
0	0.84	0.84
2	1.48	1.50
4	2.22	2.23
6	2.86	2.93

In summary, we add different U_{eff} to the strongest peak of the 4f energy level and the energy distribution range in Figure 8a–k to make it fall within the appropriate range. The energy ranges of 4f-CBM in Figure 8a–d are 2.42–2.85 eV, 2.80–3.03 eV, 2.65–3.13 eV, 2.67–2.91 eV, respectively. In Figure 8a, $\text{Ce}_{\text{Sr}1}\text{Li}_{\text{Sr}1}\text{-Sr}_2\text{Si}_5\text{N}_8$ is closer to the excitation energy range of Ce^{3+} doped $\text{Sr}_2\text{Si}_5\text{N}_8$ from 2.85 to 3.25 eV [30] reported in the experiment, but Figure 8a has a global redshift of 0.43 eV. In Figure 7e–h, the energy ranges of 4f-CBM are 2.75–2.99 eV, 2.28–3.06 eV, 2.27–3.08 eV, 2.37–2.97 eV, respectively. In Figure 8e, $\text{Pr}_{\text{Sr}1}\text{Li}_{\text{Sr}1}\text{-Sr}_2\text{Si}_5\text{N}_8$ is closer to the excitation energy range of Pr^{3+} doped SrAl_2O_4 from 2.53 to 2.88 eV [30] reported in the experiment. The energy ranges of 4f-CBM in Figure 8i–k are 2.68–3.04 eV, 2.77–3.07 eV, 2.71–3.07 eV, respectively, which is far from the experimental excitation of $\text{Sr}_2\text{Si}_5\text{N}_8:\text{Tb}^{3+}$ [16]. The U_{eff} values of Eu^{2+} and Ce^{3+} are 4 eV and 6 eV, respectively, and the energy range is mainly 2.27–2.82 eV, and the peak value is 2.27 eV, 2.39 eV, 2.82 eV. In Figure S2b, the Eu^{2+} 4f energy level is not in the forbidden band. When

Ce U_{eff} is 5 eV, the energy range of 4f-CBM is from 2.35 to 2.83 eV. The Eu^{2+} , Pr^{3+} U_{eff} values in Figure S2c are, respectively, 1 eV, 7 eV, and Eu^{2+} 4f energy levels have three strong peaks of 2.19 eV, 2.25 eV, and 2.93 eV. Pr^{3+} has the highest peak intensity of 2.69 eV in 2.69–2.99 eV.

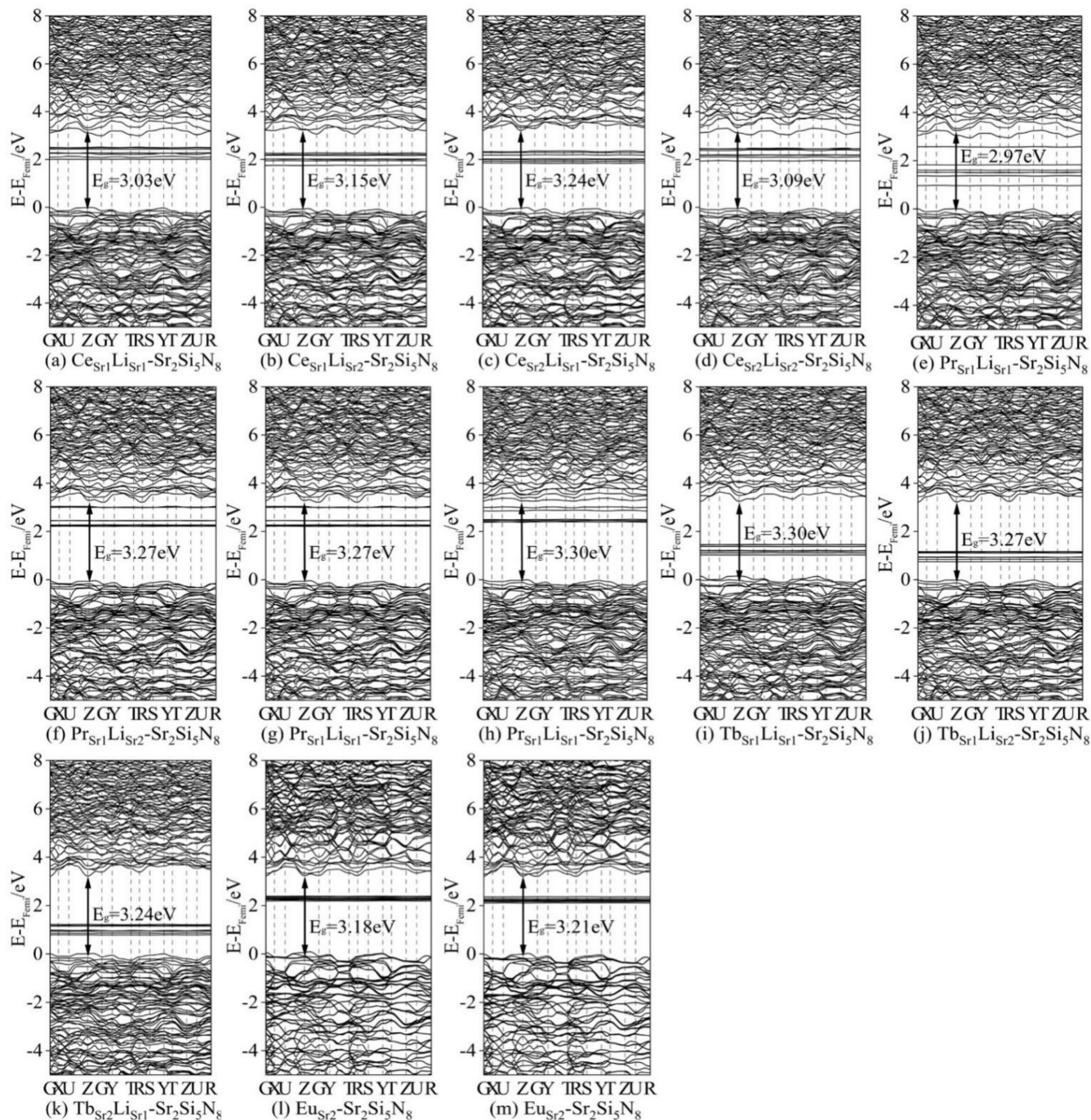


Figure 8. Band structures of doped structures: (a) $\text{Ce}_{\text{Sr}1}\text{Li}_{\text{Sr}1}\text{-Sr}_2\text{Si}_5\text{N}_8$; (b) $\text{Ce}_{\text{Sr}1}\text{Li}_{\text{Sr}2}\text{-Sr}_2\text{Si}_5\text{N}_8$; (c) $\text{Ce}_{\text{Sr}2}\text{Li}_{\text{Sr}1}\text{-Sr}_2\text{Si}_5\text{N}_8$; (d) $\text{Ce}_{\text{Sr}2}\text{Li}_{\text{Sr}2}\text{-Sr}_2\text{Si}_5\text{N}_8$; (e) $\text{Pr}_{\text{Sr}1}\text{Li}_{\text{Sr}1}\text{-Sr}_2\text{Si}_5\text{N}_8$; (f) $\text{Pr}_{\text{Sr}1}\text{Li}_{\text{Sr}2}\text{-Sr}_2\text{Si}_5\text{N}_8$; (g) $\text{Pr}_{\text{Sr}2}\text{Li}_{\text{Sr}1}\text{-Sr}_2\text{Si}_5\text{N}_8$; (h) $\text{Pr}_{\text{Sr}2}\text{Li}_{\text{Sr}2}\text{-Sr}_2\text{Si}_5\text{N}_8$; (i) $\text{Tb}_{\text{Sr}1}\text{Li}_{\text{Sr}1}\text{-Sr}_2\text{Si}_5\text{N}_8$; (j) $\text{Tb}_{\text{Sr}1}\text{Li}_{\text{Sr}2}\text{-Sr}_2\text{Si}_5\text{N}_8$; (k) $\text{Tb}_{\text{Sr}2}\text{Li}_{\text{Sr}1}\text{-Sr}_2\text{Si}_5\text{N}_8$; (l) $\text{Eu}_{\text{Sr}1}\text{-Sr}_2\text{Si}_5\text{N}_8$; (m) $\text{Eu}_{\text{Sr}2}\text{-Sr}_2\text{Si}_5\text{N}_8$.

3. Material and Methods

3.1. Theoretical Models

Three lanthanide ions ($\text{Ln}^{3+} = \text{Ce}^{3+}, \text{Pr}^{3+}, \text{Tb}^{3+}$) were selected as doping ions to dope $\text{Sr}_2\text{Si}_5\text{N}_8$ and $\text{Sr}_2\text{Si}_5\text{N}_8:\text{Eu}^{2+}$, respectively. As shown in Figure 9a, there are two kinds of Sr doping sites, namely, eight-coordinate Sr_1 [SrN_8] (0.5000, 0.8734, 0.9997) and ten-coordinate Sr_2 [SrN_{10}] (0.7500, 0.1158, 0.8683). Since in the doped ions, Ln are all positively trivalent and Sr is bivalent to neutralize the entire system's charge, every time a positive trivalent lanthanide ion is introduced to replace Sr^{2+} , a Li^+ is introduced to replace Sr^{2+} to keep the entire system electrically neutral. The chemical formula of $\text{Sr}_2\text{Si}_5\text{N}_8$ doped with $\text{Ln}^{3+}/\text{Li}^+$ is $\text{Ln}_{\text{Sr}1/\text{Sr}2}\text{Li}_{\text{Sr}1/\text{Sr}2}\text{Sr}_2\text{Si}_5\text{N}_8$, while the chemical formula of $\text{Sr}_2\text{Si}_5\text{N}_8$ doped with $\text{Ln}^{3+}/\text{Li}^+/\text{Eu}^{2+}$ is $\text{Ln}_{\text{Sr}1/\text{Sr}2}\text{Eu}_{\text{Sr}1/\text{Sr}2}\text{Li}_{\text{Sr}1/\text{Sr}2}\text{Sr}_2\text{Si}_5\text{N}_8$. Figure 9b has established a $2 \times 2 \times 1$ supercell (60 atoms) with a doping concentration of 12.5% for Ln^{3+} , Eu^{2+} , and Li^+ . If we continue to expand the unit cell to $3 \times 2 \times 1$ to reduce the doping concentration, the calculation requires more K points than $5 \times 8 \times 6$, and it is complicated for the structure to converge. Notably, $2 \times 2 \times 1$ is the largest supercell structure that can be established under the premise that the structure can converge.

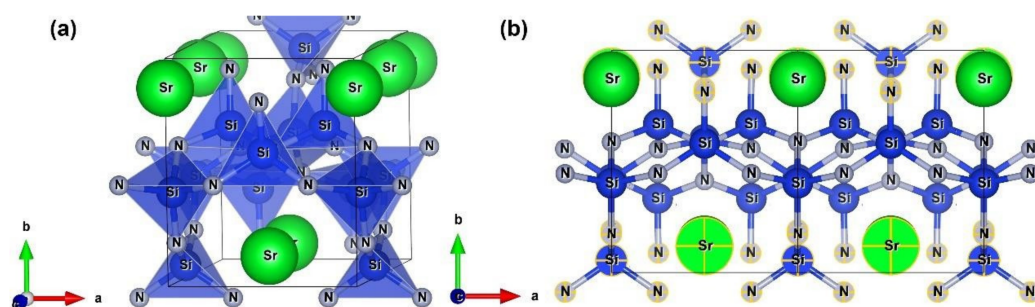


Figure 9. (a) Molecular structure of $\text{Sr}_2\text{Si}_5\text{N}_8$; (b) $2 \times 2 \times 1$ supercell of $\text{Sr}_2\text{Si}_5\text{N}_8$. The selected atoms are Sr_2 .

3.2. Computational Methods

When considering all ground-state calculations, density functional theory (DFT) calculations are performed in the Vienna AB Initio Simulation Package (VASP, Vienna ab initio simulation package) using the projector-augmented wave (PAW) method [31]. Exchange-correlation (XC, exchange-correlation) energy is described in the Perdew–Burke–Ernzerhof (PBE) method in generalized gradient approximation (GGA) [32]. The cutoff energy of all calculated plane wave bases is set to 500 eV. The energy convergence tolerance of the Self-Consistent Field (SCF) is 10^{-4} eV. The convergence tolerance of the relaxation force is 0.01 eV/Å per atom. $\text{Sr}_2\text{Si}_5\text{N}_8:\text{Eu}^{2+}$ original unit cell model removed the energy band calculation.

To solve the problem that DFT cannot handle d and f electrons, the Hubbard model compensates for the strong correlation between d and f electrons by adding additional energy terms. The corrected energy's form is as follows:

$$E^{DFT+U} = E^{DFT} + \frac{1}{2} \sum_{l,\sigma} \sum_{nl} U_{nl}^l \left[\left(n_{nl}^{l\sigma} (1 - n_{nl}^{l\sigma}) \right) \right] \quad (3)$$

There are many forms of Hubbard model correction. We choose the simplest Dudarev approximation [33]; the form is as follows:

$$\frac{(U - J)}{2} \sum_{\sigma} \left[\left(\sum_{m1} n_{m1,m1}^{\sigma} \right) - \left(\sum_{m1,m2} \hat{n}_{m1,m2}^{\sigma} \hat{n}_{m2,m1}^{\sigma} \right) \right] \quad (4)$$

U and J are the critical parameters of Hubbard's correction item, replaced by $(U - J)$. Different ions have different U_{eff} values in different host environments.

In the whole calculation process, a $5 \times 8 \times 6$ k -point network is generated using the Monkhorst–Pack method with Γ as the center. In the calculation of the energy band structure, the high-symmetry K point and the appropriate reverse spatial path are determined according to the symmetry of the crystal lattice. The electronic configuration $3s^23p^2$, $2s^2p^3$, $4s^24p^65s^2$, $2s^1$, $5s^25p^66s^24f^7$, $5s^25p^64f^15d^16s^2$, $5s^26s^25p^65d^14f^2$, and $4f^85s^26s^25p^65d^1$ correspond to Si, N, Sr, Li, Eu, Ce, Pr, and Tb in the pseudo-electron composition.

Regarding the calculation method of the effective coordination number, this article adopts Brunner's method [34], which assumes that ionic or covalent bonds connect the central atoms of the surrounding atoms. In the established $C.N$ principle, the energy standard is defined as each coordination. The bond energy between (X_i) and the central atom (M) is different from the bond energy between the nearest ligand (X_0) and the central atom. The energy ratio $E_{(M-X_i)}:E_{(M-X_0)}$ is defined as the contribution of X_i atom to M atom $C.N^*$. If the nearest atom is only affected by the Coulomb force, it is easy to get formula (5)

$$C.N_{ion}^* = \sum_i E_{(M-X_i)} / E_{(M-X_0)} = \sum_i Y_{(M-X_0)} / Y_{(M-X_i)} \quad (5)$$

where $Y_{(M-X_i)}$ is the bond length between the central atom and the ligand.

The formation of energy can evaluate the stability of the structure. The model after substitution and doping lattice can be described as the following formula (6):

$$E_f(\text{Sr}_2\text{Si}_5\text{N}_8:\text{Eu}^{2+}/\text{Ln}^{3+}/\text{Li}^+) = E(\text{Sr}_2\text{Si}_5\text{N}_8:\text{Eu}^{2+}/\text{Ln}^{3+}/\text{Li}^+) + 3\mu(\text{Sr}^{2+}) - E(\text{Sr}_2\text{Si}_5\text{N}_8) - \mu(\text{Eu}^{2+}) - \mu(\text{Ln}^{3+}) - \mu(\text{Li}^+) \quad (6)$$

In the above formula $E_f(\text{Sr}_2\text{Si}_5\text{N}_8:\text{Eu}^{2+}/\text{Ln}^{3+}/\text{Li}^+)$ is the formation energy, $E(\text{Sr}_2\text{Si}_5\text{N}_8:\text{Eu}^{2+}/\text{Ln}^{3+}/\text{Li}^+)$ is the energy calculated by SCF, $\mu(\text{Sr}^{2+})$, $\mu(\text{Eu}^{2+})$, $\mu(\text{Li}^+)$ are the chemical potentials of Sr, Eu, Li, and Ln, respectively, and $E(\text{Sr}_2\text{Si}_5\text{N}_8)$ is the energy calculated by the lattice matrix SCF. For the chemical potential of the element, formula (7) can be used

$$\mu(x) = E(\text{Cell of } X) / n \quad (7)$$

where $\mu(x)$ is the chemical potential of X , $E(\text{Cell of } X)$ is the elemental unit cell of element X , and n is the number of X contained in the elemental unit cell.

4. Conclusions

In this study, two models of $\text{Sr}_2\text{Si}_5\text{N}_8:\text{Ln}^{3+}/\text{Li}^+$ and $\text{Sr}_2\text{Si}_5\text{N}_8:\text{Ln}^{3+}/\text{Eu}^{2+}/\text{Li}^+$ were constructed. The calculation of $\text{Sr}_2\text{Si}_5\text{N}_8:\text{Ln}^{3+}/\text{Li}^+$ and $\text{Sr}_2\text{Si}_5\text{N}_8:\text{Eu}^{2+}$ provides a basic reference for double-doped lanthanide ions. The introduction of Li^+ and Ln^{3+} can achieve the design idea of neutralizing electrons and maintaining the original structure. Three dual-doped models of $\text{Eu}_{\text{Sr}1}\text{Ce}_{\text{Sr}1}\text{Li}_{\text{Sr}2}-\text{Sr}_2\text{Si}_5\text{N}_8$, $\text{Eu}_{\text{Sr}2}\text{Ce}_{\text{Sr}1}\text{Li}_{\text{Sr}2}-\text{Sr}_2\text{Si}_5\text{N}_8$, and $\text{Eu}_{\text{Sr}2}\text{Pr}_{\text{Sr}2}\text{Li}_{\text{Sr}2}-\text{Sr}_2\text{Si}_5\text{N}_8$ were screened out. Among the three models mentioned, $\text{Eu}_{\text{Sr}1}\text{Ce}_{\text{Sr}1}\text{Li}_{\text{Sr}2}-\text{Sr}_2\text{Si}_5\text{N}_8$ and $\text{Eu}_{\text{Sr}2}\text{Pr}_{\text{Sr}2}\text{Li}_{\text{Sr}2}-\text{Sr}_2\text{Si}_5\text{N}_8$'s fluorescence performances are expected to exceed that of $\text{Sr}_2\text{Si}_5\text{N}_8:\text{Eu}^{2+}$, which can be regarded as a potential route to increase the quenching temperature of the phosphor. When Ce^{3+} U_{eff} in $\text{Ce}_{\text{Sr}1}\text{Li}_{\text{Sr}1}-\text{Sr}_2\text{Si}_5\text{N}_8$ is 5 eV, the energy range of 4f-CBM is 2.42–2.85 eV. Compared with the experimentally reported excitation range of 2.85–3.25 eV, the redshift is 0.42 eV (75 nm). When Pr^{3+} U_{eff} in $\text{Pr}_{\text{Sr}1}\text{Li}_{\text{Sr}1}-\text{Sr}_2\text{Si}_5\text{N}_8$ is 4 eV, the energy range of 4f-CBM is 2.75–2.99 eV, and its peak value is 2.90 eV, which is similar to $\text{SrAl}_2\text{O}_4:\text{Pr}^{3+}$ 430–490nm with peaks around 440 nm. In $\text{Sr}_2\text{Si}_5\text{N}_8:\text{Ln}^{3+}/\text{Li}^+/\text{Eu}^{2+}$, three convergent models of $\text{Eu}_{\text{Sr}1}\text{Ce}_{\text{Sr}1}\text{Li}_{\text{Sr}1}-\text{Sr}_2\text{Si}_5\text{N}_8$, $\text{Eu}_{\text{Sr}2}\text{Ce}_{\text{Sr}1}\text{Li}_{\text{Sr}1}-\text{Sr}_2\text{Si}_5\text{N}_8$, and $\text{Eu}_{\text{Sr}2}\text{Pr}_{\text{Sr}2}\text{Li}_{\text{Sr}1}-\text{Sr}_2\text{Si}_5\text{N}_8$ were selected. The addition of Ce^{3+} in $\text{Eu}_{\text{Sr}1}\text{Ce}_{\text{Sr}1}\text{Li}_{\text{Sr}1}-\text{Sr}_2\text{Si}_5\text{N}_8$ made the 4f energy level of Eu^{2+} blue shift. Similarly, the addition of Pr^{3+} in $\text{Eu}_{\text{Sr}2}\text{Pr}_{\text{Sr}2}\text{Li}_{\text{Sr}1}-\text{Sr}_2\text{Si}_5\text{N}_8$ makes part of the Eu^{2+} 4f energy level blue shift. The Eu^{2+} 4f energy level in $\text{Eu}_{\text{Sr}2}\text{Ce}_{\text{Sr}1}\text{Li}_{\text{Sr}1}-\text{Sr}_2\text{Si}_5\text{N}_8$ is not in the forbidden band, so Eu^{2+} is not used as the emission center.

Supplementary Materials: The following are available online. Figure S1: Density of states of doped structures: (a) $\text{Ce}_{\text{Sr}1}\text{Li}_{\text{Sr}1}-\text{Sr}_2\text{Si}_5\text{N}_8$; (b) $\text{Ce}_{\text{Sr}1}\text{Li}_{\text{Sr}2}-\text{Sr}_2\text{Si}_5\text{N}_8$; (c) $\text{Ce}_{\text{Sr}2}\text{Li}_{\text{Sr}1}-\text{Sr}_2\text{Si}_5\text{N}_8$; (d) $\text{Ce}_{\text{Sr}2}\text{Li}_{\text{Sr}2}-\text{Sr}_2\text{Si}_5\text{N}_8$; (e) $\text{Pr}_{\text{Sr}1}\text{Li}_{\text{Sr}1}-\text{Sr}_2\text{Si}_5\text{N}_8$; (f) $\text{Pr}_{\text{Sr}1}\text{Li}_{\text{Sr}2}-\text{Sr}_2\text{Si}_5\text{N}_8$; (g) $\text{Pr}_{\text{Sr}2}\text{Li}_{\text{Sr}1}-\text{Sr}_2\text{Si}_5\text{N}_8$; (h)

PrSr₂LiSr₂-Sr₂Si₅N₈; (i) TbSr₁LiSr₁-Sr₂Si₅N₈; (j) TbSr₁LiSr₂-Sr₂Si₅N₈; (k) TbSr₁LiSr₂-Sr₂Si₅N₈; (l) EuSr₁-Sr₂Si₅N₈; (m) EuSr₂-Sr₂Si₅N₈. Figure S2: Density of states of doped structures: (a) EuSr₁CeSr₁LiSr₂-Sr₂Si₅N₈; (b) EuSr₂CeSr₁LiSr₂-Sr₂Si₅N₈; (c) PrSr₂EuSr₂LiSr₂-Sr₂Si₅N₈. Table S1: The Key information in the energy band structure of Sr₂Si₅N₈:Ln³⁺/Li⁺, Eu²⁺. Table S2: The Key information in the energy band structure of Sr₂Si₅N₈:Ln³⁺/Li⁺/Eu²⁺.

Author Contributions: Conceptualization, Z.Y., Q.S. and J.Z.; formal analysis, Z.Y.; software, Z.Y. and J.Z.; funding acquisition, M.L. and Q.S.; investigation, Z.Y. and J.Z.; methodology, Z.Y. and J.Z.; project administration, Z.Y. and M.L.; supervision, Z.Y., Q.S. and M.L.; writing—original draft, Z.Y.; writing—review and editing, Z.Y. and M.L. All authors have read and agreed to the published version of the manuscript.

Funding: The National Natural Science Foundation of China (Nos. 51872217 and 51521001), the “111” Project (No. B13035).

Institutional Review Board Statement: Not applicable.

Informed Consent Statement: Not applicable.

Data Availability Statement: The data that support the findings of this study are available from the corresponding authors upon reasonable request.

Conflicts of Interest: The authors declare that they have no known competing financial interests or personal relationships that could have appeared to influence the work reported in this paper.

Sample Availability: The samples of compounds are not available from authors.

References

1. Li, Y.Q.; van Steen, J.E.J.; van Krevel, J.W.H.; Botty, G.; Delsing, A.C.A.; DiSalvo, F.J.; de With, G.; Hintzen, H.T. Luminescence properties of red-emitting M₂Si₅N₈:Eu²⁺ (M = Ca, Sr, Ba) LED conversion phosphors. *J. Alloys Compd.* **2006**, *417*, 273–279. [[CrossRef](#)]
2. Liu, Y.H.; Chen, L.; Zhou, X.F.; Liu, R.H.; Zhuang, W.D. Structure, luminescence and thermal quenching properties of Eu doped Sr_{2-x}Ba_xSi₅N₈ red phosphors. *J. Solid State Chem.* **2016**, *246*, 145–149. [[CrossRef](#)]
3. Chen, L.; Liu, R.-H.; Zhuang, W.-D.; Liu, Y.-H.; Hu, Y.-S.; Du, F. Effect of Eu²⁺ concentration on the thermal quenching mechanism of Sr₂Si₅N₈:Eu²⁺ red phosphors. *Chin. J. Lumin.* **2015**, *36*, 371–376. [[CrossRef](#)]
4. Seibald, M.; Rosenthal, T.; Oeckler, O.; Maak, C.; Tücks, A.; Schmidt, P.J.; Wiechert, D.; Schnick, W. New polymorph of the highly efficient LED-phosphor SrSi₂O₂N₂: Eu²⁺-polytypism of a layered oxonitridosilicate. *Chem. Mater.* **2013**, *25*, 1852–1857. [[CrossRef](#)]
5. Chen, L.; Liu, R.H.; Zhuang, W.D.; Liu, Y.H.; Hu, Y.S.; Zhou, X.F.; Ma, X.L. A study on photoluminescence and energy transfer of SrAlSi₄N₇: Eu²⁺, Ce³⁺ phosphors for application in white-light LED. *J. Alloys Compd.* **2015**, *627*, 218–221. [[CrossRef](#)]
6. Daicho, H.; Shinomiya, Y.; Enomoto, K.; Nakano, A.; Sawa, H.; Matsuiishi, S.; Hosono, H. A novel red-emitting K₂Ca(PO₄)F:Eu²⁺ phosphor with a large Stokes shift. *Chem. Commun.* **2018**, *54*, 884–887. [[CrossRef](#)] [[PubMed](#)]
7. Shang, M.M.; Li, C.X.; Lin, J. ChemInform abstract: How to produce white light in a single-phase host? *ChemInform* **2014**, *43*, 1372–1386.
8. Dorenbos, P. A review on how Lanthanide impurity levels change with chemistry and structure of inorganic compounds. *ECS J. Solid State Sci. Technol.* **2013**, *2*, R3001–R3011.
9. Li, Y.Q.; de With, G.; Hintzen, H.T. The effect of replacement of Sr by Ca on the structural and luminescence properties of the red-emitting Sr₂Si₅B₈:Eu²⁺ LED conversion phosphor. *J. Solid State Chem.* **2008**, *181*, 515–524.
10. Bulloni, C.; García-Fuente, A.; Umland, W.; Daul, C. Effect of Ca²⁺ codoping on the Eu²⁺ luminescence properties in the Sr₂Si₅N₈:Eu²⁺ host lattice: A theoretical approach. *Phys. Chem. Chem. Phys.* **2015**, *17*, 24925–24930. [[CrossRef](#)]
11. Chen, L.; Liu, R.H.; Zhuang, W.D.; Liu, Y.H.; Hu, Y.S.; Zhou, X.F.; Gao, W.; Ma, X.L. Structure, photoluminescence, and thermal quenching properties of Eu doped Sr₂Al_xSi_{5-x}N_{8-x/3} red phosphors. *CrystEngComm* **2015**, *17*, 3687–3694. [[CrossRef](#)]
12. Wang, T.; Zheng, P.; Liu, X.L.; Chen, H.F.; Bian, L.; Liu, Q.L. Effects of replacement of AlO⁺ for SiN⁺ on the structure and optical properties of Sr₂Si₅N₈:Eu²⁺ phosphors. *J. Lumin.* **2014**, *147*, 173–178. [[CrossRef](#)]
13. Qiao, J.; Ning, L.; Molochev, M.S.; Chuang, Y.C.; Zhang, Q.; Poeppelmeier, K.R.; Xia, Z. Site-Selective Occupancy of Eu²⁺ Toward Blue-Light-Excited Red Emission in a Rb₃YSi₂O₇:Eu Phosphor. *Angew. Chem. Int. Ed.* **2019**, *131*, 11645–11650.
14. Li, H.; Li, W.; Liu, X.; Ren, C.; Miao, X.; Li, X. Engineering of Gd/Er/Lu-triple-doped Bi₂MoO₆ to synergistically boost the photocatalytic performance in three different aspects: Oxidizability, light absorption and charge separation. *Appl. Surf. Sci.* **2019**, *463*, 556–565. [[CrossRef](#)]
15. Tang, W.; Ding, S.; Yuan, Y.; Xie, G. Effect of Ce³⁺ and Tb³⁺ codoping on luminescence properties of Na₃SrMg₁₁(PO₄)₉:Eu²⁺ phosphors. *Opt. Mater.* **2020**, *106*, 110003. [[CrossRef](#)]
16. Peng, X.; Li, S.-X.; Liu, X.-J.; Huang, Y.-H.; Huang, Z.-R.; Li, H.-L. Syntheses and photoluminescence properties of Eu²⁺/Tb³⁺ doped Sr₂Si₅N₈ phosphors. *J. Inorg. Mater.* **2015**, *30*, 397–400.

17. Li, H.L.; Liu, X.J.; Huang, L.P. Luminescent properties of Luag: Ce phosphors with different ce contents prepared by a sol-gel combustion method. *Opt. Mater.* **2007**, *29*, 1138–1142. [[CrossRef](#)]
18. Zorenko, Y.; Gorbenko, V.; Voznyak, T.; Zorenko, T.; Kuklinski, B.; Turos-Matysyak, R.; Grinberg, M. Luminescence properties of phosphors based on Tb₃Al₅O₁₂ (TbAG) terbium-aluminum garnet. *Opt. Spectrosc.* **2009**, *106*, 365–374. [[CrossRef](#)]
19. Zhong, J.Y.; Zhao, W.R.; Du, F.; Wen, J.; Zhuang, W.D.; Liu, R.H.; Duan, C.-K.; Wang, L.G.; Lin, K. Identifying the emission centers and probing the mechanism for highly efficient and thermally stable luminescence in the La₃Si₆N₁₁: Ce³⁺ Phosphor. *J. Phys. Chem. C* **2018**, *122*, 7849–7858. [[CrossRef](#)]
20. Li, Y.Q.; de With, D.; Hintzen, H.T. Luminescence properties of Ce³⁺-activated alkaline earth silicon nitride M₂Si₅N₈ (M=Ca, Sr, Ba) materials. *J. Lumin.* **2006**, *116*, 107–116.
21. Pust, P.; Wochnik, A.S.; Baumann, E.; Schmidt, P.J.; Wiechert, D.; Scheu, C.; Schnick, W. Ca[LiAl₃N₄]: Eu²⁺—A narrow-band red-emitting nitridolithoaluminate. *Chem. Mater.* **2014**, *26*, 3544–3549.
22. Wilhelm, D.; Baumann, D.; Seibald, M.; Wurst, K.; Heymann, G.; Huppertz, H. Narrow-band red emission in the nitridolithoaluminate Sr₄[LiAl₁₁N₁₄]: Eu²⁺. *Chem. Mater.* **2017**, *29*, 1204–1209. [[CrossRef](#)]
23. Strobel, P.; Weiler, V.; Hecht, C.; Schmidt, P.J.; Schnick, W. Luminescence of the narrow-band red emitting nitridomagnesiumsilicate Li₂(Ca_{1-x}Sr_x)₂[Mg₂Si₂N₆]: Eu²⁺ (x = 0 – 0.06). *Chem. Mater.* **2017**, *29*, 1377–1383. [[CrossRef](#)]
24. Fang, C.M.; Hintzen, H.T.; de With, G.; de Groot, R.A. Electronic structure of the alkaline-earth silicon nitrides M₂Si₅N₈ (M=Ca and Sr) obtained from first-principles calculations and optical reflectance spectra. *J. Phys. Condens. Matter* **2001**, *13*, 67–76.
25. Shen, T.-Y.; Wu, Y.; Shen, Y.-F.; Zou, Z.-G.; Zhang, F.; Long, Z.-J. Photophysical properties and electronic structure of Sr₂Si₅N₈:Eu²⁺. *J. Synth. Cryst.* **2014**, *43*, 1212–1216.
26. Xi, Q. Research on Ionic Radius. *J. Hainan Norm. Univ.* **2001**, *14*, 68–75.
27. Zhang, L.G.; Jin, H.; Yang, W.Y.; Xie, Z.P.; Miao, H.Z.; An, L. Optical properties of single-crystalline alpha-Si₃N₄ nanobelts. *Appl. Phys. Lett.* **2005**, *86*, 061908. [[CrossRef](#)]
28. Sikander, A.; Muhammad, I.; Ayaz, K.S.; Ali, Z.; Kityk, I.V.; Muhammad, S.; Al-Sehemi, A.G. Doping induced effect on optical and band structure properties of Sr₂Si₅N₈ based phosphors: DFT approach. *J. Alloy. Compound.* **2019**, *771*, 1072–1079. [[CrossRef](#)]
29. Ten Kate, O.M.; Zhang, Z.; Dorenbos, P.; Hintzen, H.T.; Van der Kolk, E. 4f and 5d energy levels of the divalent and trivalent lanthanide ions in M₂Si₅N₈ (M=Ca, Sr, Ba). *J. Solid State Chem.* **2013**, *197*, 209–217. [[CrossRef](#)]
30. Chawla, S.; Kumar, N.; Chander, H. Broad yellow orange emission from SrAl₂O₄:Pr³⁺ phosphor with blue excitation for application to white LEDs. *J. Lumin.* **2009**, *129*, 114–118. [[CrossRef](#)]
31. Kresse, G.; Furthmüller, J. Efficiency of ab-initio total energy calculations for metals and semiconductors using a plane-wave basis set. *Comput. Mater. Sci.* **1996**, *6*, 15–50. [[CrossRef](#)]
32. Dufek, P.; Blaha, P.; Sliwko, V.; Schwarz, K. Generalized-gradient-approximation description of band splittings in transition-metal oxides and fluorides. *Phys. Rev. B Condens. Matter* **1994**, *49*, 10170–10175. [[CrossRef](#)] [[PubMed](#)]
33. Dudarev, S.L.; Botton, G.A.; Savrasov, S.Y.; Humphreys, C.J.; Sutton, A.P. Electron-energy-loss spectra and the structural stability of nickel oxide: An LSDA+U study. *Phys. Rev. B* **1998**, *57*, 1505–1509. [[CrossRef](#)]
34. Guo, H.; Wu, Q. The calculation method of effective coordination number. *J. Shenyang Univ. Chem. Technol.* **1991**, *4*, 245.